

BIELEFELD UNIVERSITY

MASTERS THESIS

---

# Simulating sedation-induced unconsciousness in a Neural-Mass-Model

---

*Author:*  
Felix FRIESE

*Supervisor:*  
Dr. Malte SCHILLING

*Examiner:*  
Prof Dr. Helge RITTER

*A thesis submitted in fulfillment of the requirements  
for the degree of Master of Science  
in the*

Neuroinformatics Groups  
Faculty of Technology

May 29, 2022



BIELEFELD UNIVERSITY

# *Abstract*

Faculty of Technology  
Neuroinformatics Groups

Master of Science

## **Simulating sedation-induced unconsciousness in a Neural-Mass-Model**

by Felix FRIESE

Patients with severe Traumatic Brain Injuries (TBI) often remain in a state of unresponsive wakefulness. Brain-Computer-Interface (BCI)-based systems promise to improve the state assessment and to open a communication channel for patients to express their intent while in conscious states. Developing such a BCI-System (e.g. with EEG), including the necessary algorithms to assess a patients current wakefulness or consciousness state from EEG data is a challenging task. Development, testing and evaluation of these algorithms requires labeled data (ground truth), which is almost impossible to obtain given the patients' lack of communication capabilities. Therefore, it would be desirable to generate a synthetic signal, which should ideally resemble real EEG data in all relevant features.

We previously developed a simple ICA-based model, which generates a multichannel EEG from base-signals with configurable spectral features. While this proved useful for testing numerous components of our signal-analysis framework, it lacks biological plausibility and explanatory power to model the changes in the signal's properties given an altered state of consciousness.

In this thesis, we propose an approach towards overcoming these issues while sticking with the original goal of generating realistic, practically useful surrogate data. A biologically motivated Neural Mass Model (NMM) on cortical-column level is implemented, which is able to approximate the effects of sedation-induced unconsciousness on the generated signal. The model is then shown to be able to reproduce the characteristic effects that sedation has on the EEG-Signals of real subjects. This is a first step to a model of consciousness-altering processes in the brain, which could ultimately be extended to realistically simulate other processes like sleep and trauma-induced DoC, facilitating better detection algorithms and furthering the goal to develop working BCI-Systems in the given context.



# Contents

<b>Abstract</b>	<b>iii</b>
<b>1 Introduction</b>	<b>1</b>
1.1 Motivation Deutsch . . . . .	1
1.2 Related Work . . . . .	2
1.3 Collection of Quotes . . . . .	2
<b>2 Technical Concepts</b>	<b>3</b>
2.1 States of Consciousness . . . . .	3
2.1.1 Definition . . . . .	3
2.1.2 State Transitions . . . . .	3
2.1.2.1 Natural Transitions . . . . .	3
2.1.2.2 Sedation . . . . .	3
2.1.3 Disorders of Consciousness . . . . .	3
2.2 EEG . . . . .	4
2.2.1 Measurement . . . . .	4
2.2.2 Advantages/Disadvantages . . . . .	4
2.2.3 States of Consciousness in the EEG Signal . . . . .	4
2.2.3.1 State Detection in healthy Subjects . . . . .	4
2.2.3.2 State Detection in Subjects with DOC . . . . .	4
2.2.4 Simulation . . . . .	4
2.2.4.1 Motivation . . . . .	4
2.2.4.2 Approaches . . . . .	4
2.2.4.3 Model Choice . . . . .	4
2.3 Neural Mass Models . . . . .	5
2.3.1 The Jansen-Rit Model . . . . .	5
2.3.1.1 Potential-To-Rate Block . . . . .	6
2.3.1.2 PSP-Blocks . . . . .	7
2.3.1.3 Full Linear System . . . . .	10
2.3.1.4 Connectivity Constants . . . . .	11
2.3.1.5 Model Input . . . . .	11
2.3.1.6 Model Output . . . . .	11
2.3.2 The David and Friston Model . . . . .	13
2.3.2.1 Introducing sub-populations . . . . .	13
2.3.3 New PSP Functions . . . . .	15
<b>3 Methodology</b>	<b>17</b>
3.1 PyRates Framework . . . . .	17
3.1.1 Network Representations . . . . .	18
3.1.1.1 YAML Representation . . . . .	18
3.1.1.2 Python Representation . . . . .	19

3.1.2	Implementation of the Jansen-Rit Model . . . . .	19
3.1.3	Simulating GABA-A Sedatives . . . . .	21
<b>4</b>	<b>Results</b>	<b>23</b>
4.1	Research Results . . . . .	23
4.1.1	Units for propofol concentration . . . . .	23
4.1.2	Realistic propofol concentrations during general anaesthesia (GA)	23
4.1.3	Effects of propofol on the IPSP . . . . .	23
4.1.4	Hysteresis of propofol . . . . .	24
4.1.5	Biphasic Effect . . . . .	25
4.2	Simulating Propofol in the System . . . . .	25
4.3	Simulating over the parameter space . . . . .	26
4.4	Discussion . . . . .	27
	<b>Bibliography</b>	<b>29</b>

# List of Abbreviations

<b>NMM</b>	<b>N</b> eural <b>M</b> ass <b>M</b> odel
<b>DoC</b>	<b>D</b> isorder of <b>C</b> onsciousness
<b>TBI</b>	<b>T</b> raumatic <b>B</b> rain <b>I</b> njury
<b>BCI</b>	<b>B</b> rain <b>C</b> omputer <b>I</b> nterface
<b>ICA</b>	<b>I</b> ndependent <b>C</b> omponent <b>A</b> nalysis
<b>PSP</b>	<b>P</b> ost- <b>S</b> ynaptic- <b>P</b> otential
<b>EPSP</b>	<b>E</b> xcitatory <b>P</b> ost- <b>S</b> ynaptic- <b>P</b> otential
<b>IPSP</b>	<b>I</b> nhibitory <b>P</b> ost- <b>S</b> ynaptic- <b>P</b> otential
<b>GABA</b>	<b>G</b> amma- <b>A</b> minobutyric <b>A</b> cid
<b>EEG</b>	<b>E</b> lectroencephalography
<b>PC</b>	<b>P</b> yramidal <b>C</b> ell
<b>EIN</b>	<b>E</b> xcitatory <b>I</b> nter <b>n</b> euron
<b>IIN</b>	<b>I</b> nhibitory <b>I</b> nter <b>n</b> euron





# Chapter 1

## Introduction

### 1.1 Motivation Deutsch

Die hochkomplexen Prozesse der Änderung von Bewusstseinszuständen im menschlichen Gehirn sind nach wie vor kaum verstanden. Die Definition und Feststellung von Bewusstseinszuständen beruht in der Praxis weiterhin stark auf Verhaltensbasierten Beobachtungen (e.g. Reiz-Reaktions Tests) [\[hier möglicherweise Glasgow Coma Scale erwähnen\]](#). Insbesondere bei Menschen die unter traumatischen Hirnschädigungen leiden, ist diese Herangehensweise jedoch unzureichend, da die Gründe für ausbleibende externe Reaktionen vielseitig sein können. Daher werden zunehmend Messungen der Hirnaktivität durch Neuroimaging (fMRT, EEG, ...) herangezogen um Bewusstseinszustände zu bestimmen und zu erforschen, sowie bestimmte Zustandsgrenzen neu zu definieren. Dabei gibt es bereits beeindruckende Erfolge, wie beispielsweise eine basale Kommunikation über BCI-Systeme mit Trauma-Patienten die über keinerlei äußerlich erkennbare Regung als aufmerksam zu erkennen gewesen wären. Die genauen Mechanismen hinter Zustandsänderungen sowie klare objektive Grenzen zwischen Zuständen sind aber immer noch der Gegenstand von Grundlagenforschung. Ein Ansatz um Stück für Stück bessere Einsicht in diese Prozesse zu erlangen, ist die Computer-Simulation von kontrollierten Zustandsveränderungen, beispielsweise einer Anästhesie, um ein Verständnis für die Veränderung von Dynamiken der Gehirnaktivität und deren Auswirkungen zu entwickeln. Das Betäubungsmittel Propofol wird in der Medizin verwendet um im kontrollierten Rahmen einen völligen Bewusstseinsverlust zur Durchführung von Operationen herbeizuführen. Der neurochemische Wirkmechanismus von Propofol auf synaptische Rezeptoren ist bereits gut erforscht und bietet eine solide Grundlage für die Erforschung von Sedationsprozessen. Diese Arbeit beschäftigt sich mit der Möglichkeit diese Wirkmechanismen auf Computermodelle von Neuronenpopulationen im Gehirn anzuwenden und das entstehende Verhalten des Systems zu analysieren sowie Vergleiche zu den bisherigen neurologischen Erkenntnissen im Bereich Anästhesie zu ziehen. Ein gängiges Messverfahren um Anästhesie zu beobachten ist das EEG, das insbesondere wegen seines non-invasiven, portablen und relativ kostengünstigen Einsatzes Verwendung findet. Als Modell zur Simulation von EEG-ähnlichen Signalen bieten sich sogenannte Neural-Mass-Models (NMMs) an, die sich auf die Modellierung der Dynamiken von größeren Neuronenpopulationen fokussieren.

## 1.2 Related Work

There have been many efforts to simulate different states of consciousness with NMMs. A particularly sophisticated example is Bensaïd et al.'s COALIA Framework [23], which is able to produce realistic resting-state EEG-like signals for sleep and wakefulness, by using the output of over 60 interconnected NMMs and applying a transformation onto scalp electrodes using a realistic head-model with tissue conductivities. Liang et al. [19] focussed on relating propofol-induction to effect-site concentration, which is an important parameter in any model for anaesthesia-simulation.

## 1.3 Collection of Quotes

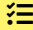
'Although our understanding of the actions of propofol at the molecular level is quite extensive, we do not entirely understand how these molecular effects translate into alterations in cellular, synaptic and neural network function, and in turn cause unconsciousness [88]. This knowledge gap is, at least in part, the result of a lack of a generally accepted theory of consciousness. In recent years, cognitive neuroscience has seen a resurgence of interest in this topic, with attempts to integrate anaesthesia and sleep research in order to address this deficiency. This resurgence has revealed several brain areas that play a crucial role in generation of consciousness, and which are extensively influenced by hypnotic drugs.' [21]

## Chapter 2

# Technical Concepts

### 2.1 States of Consciousness

#### 2.1.1 Definition


 **Todo** which states of consciousness are commonly defined

- How do we define States of Consciousness?
- What do we know about them (and what do we not)?
  - How do these states change (naturally)?
  - What has an influence on the state?
  - What happens for DOCs?

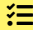
[27]

#### 2.1.2 State Transitions


##### 2.1.2.1 Natural Transitions

 **Todo** how states transition into each other naturally

##### 2.1.2.2 Sedation

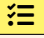
 **Todo** how sedation differs from natural loss of consciousness

#### 2.1.3 Disorders of Consciousness

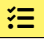
 **Todo** the symptoms of DOCs

## 2.2 EEG

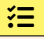
### 2.2.1 Measurement

 **Todo** how the EEG is measured technically and which neuronal processes it actually observes (signal amplification, pyramidal cells, ...)

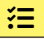
### 2.2.2 Advantages/Disadvantages

 **Todo** spatial/temporal resolution, invasiveness, ...

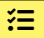
### 2.2.3 States of Consciousness in the EEG Signal

 **Todo** how do the states differ in the signal

#### 2.2.3.1 State Detection in healthy Subjects

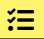
 **Todo** rough explanation of prevalent algorithms

#### 2.2.3.2 State Detection in Subjects with DOC


 **Todo** issues with data collection, structurally different source signal, ...

### 2.2.4 Simulation

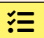
#### 2.2.4.1 Motivation

 **Todo** what can we hope to achieve by simulating an EEG signal

#### 2.2.4.2 Approaches

 **Todo** which tools are at our disposal (naive frequency mixing, population models, simulating individual neurons, ...)

#### 2.2.4.3 Model Choice

 **Todo** argue about models  $\Rightarrow$  why did we land on NMMs/population models?

## 2.3 Neural Mass Models

**Todo** slightly deeper introduction (we already have this in the EEG section) to NMMs in general

### 2.3.1 The Jansen-Rit Model

The widely used Jansen-Rit Model [5], [6], is based on earlier models by Wilson & Cowan [1], Lopes da Silva et al. [2], [3] and Zetterberg et al. [4]. It represents a cortical column in the brain, which is made up of three main components, each modeling a population of neurons with distinct characteristics.

The basic schema of the model is visualized in Fig. 2.1, showing the connections between the main components. There is a population of Pyramidal Cells which receives input from two populations of inter-neurons, one of which is excitatory while the other is inhibitory. Each of the inter-neuron-populations receives the output of the PC population. Additionally, there is external excitatory input to the PC population from other regions of the brain.

The Block Diagram (Fig. 2.2) shows the individual modules of the model. A population consists of two types of blocks: The *PSP-Block* models the behavior of the synapses and neuronal somata. It can be either excitatory or inhibitory and converts the incoming average pre-synaptic pulse density to an average post-synaptic membrane potential by convolving it with an impulse response function ( $h_e(t)$  and  $h_i(t)$ , for excitation and inhibition respectively). The second block (sometimes called *Potential-To-Rate-Block* after it's functionality) calculates the populations response to this stimulation, transforming the incoming average membrane potential back into an average pulse density of action potentials. It may be roughly viewed as a functional counterpart to the axon hillock by establishing a firing threshold and is usually implemented by a Sigmoid Function (*Sigm*). External input from other regions of the brain is represented by  $p(t)$ . The Connectivity Constants  $C_1$ ,  $C_2$ ,  $C_3$  and  $C_4$  are a proportional representation of the average number of synapses between the populations. The signal most closely related to the EEG and therefore the variable of interest, is the summed average membrane potential of the PC population ( $y_1(t) - y_2(t)$  in Fig. 2.2).

**Todo** explain neurophysiology why  $EEG \approx y_1 - y_2$ , or reference back to explanation in EEG section

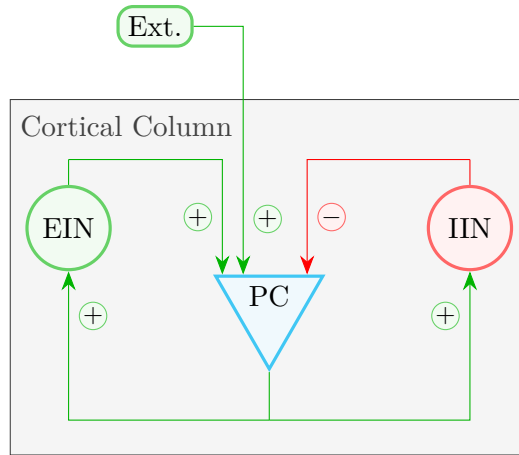
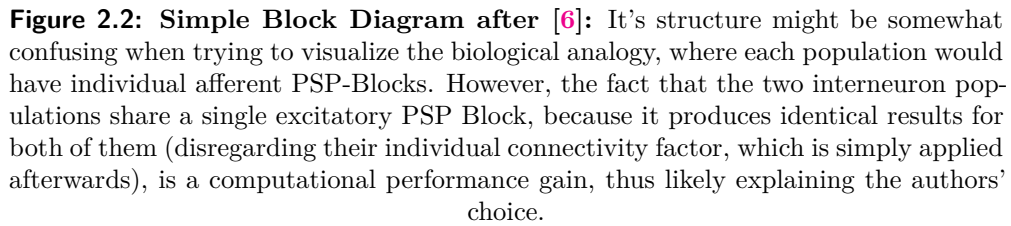


**Figure 2.1: Basic Schema of the Jansen-Rit Model:** Three populations of neurons



For a neuron to fire an action potential, its membrane potential needs to surpass a certain threshold. Since we are modeling not a single neuron but a whole population, we need an operator that can transform the mean membrane potential that the neurons of the population receive as input into an average firing rate for the whole population. While neurons within the population may have individual firing-thresholds, it can be assumed due to their sheer number, that these thresholds are normally distributed around some mean value  $v_0$ . An additional assumption that this approach rests on, is that the number of afferent (i.e. incoming) connections to the individual neurons is sufficiently large to justify the assertion that all neurons receive roughly the same stimulation. This must be modeled by a monotonically increasing function. The Potential-To-Rate Block represents this process with a Sigmoid. After multiple iterations by Zetterberg [4], Lopes da Silva [3] and others, Jansen and Rit [5], [6] landed on the following equation:

The parameter values (Table 2.1) are empirically determined [5]. The maximum firing rate the population can achieve is set at  $5\text{Hz}$ . A mean membrane potential of  $6\text{mV}$  (equal to the populations average firing threshold) elicits half of the maximum firing rate, while  $\frac{0.56}{\text{mV}}$  defines the steepness. The plot in Fig. 2.3 visualizes these properties.

**Table 2.1:** Parameters of the Sigmoid Function

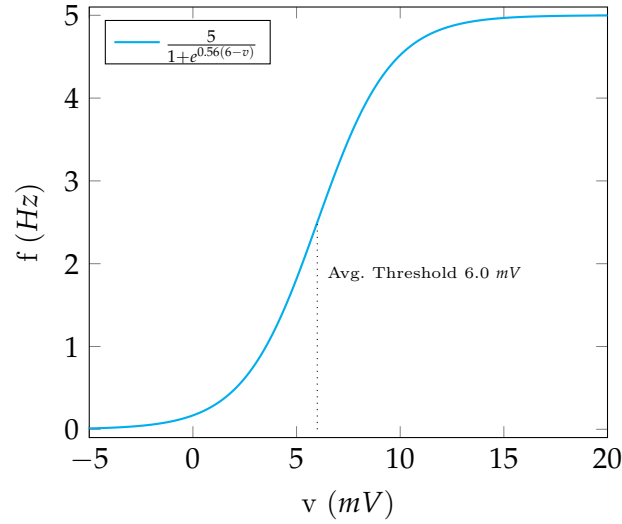


**Figure 2.3:** Sigmoid (Eq. 2.1) [5]

### 2.3.1.2 PSP-Blocks

In Physics, Linear Time-Invariant Systems (LTI systems) are oftentimes used to describe the response of electrical circuits to arbitrary input signals. They consist of a kernel function (or impulse-response function), that models the system's response to a single unit-impulse. The PSP-Blocks are an LTI system, fully represented by an impulse response function. It describes a PSP relative to the onset of a pulse. Since the PSP differs depending on the type of cell (excitatory or inhibitory), there are two different impulse-response functions. The parameters for the EPSP (Eq. 2.2) and IPSP (Eq. 2.3) are given in Table 2.2. The respective plots are visualized in Fig. 2.4.

Parameter		Default Value	Unit
Excmaxamplitude / $e$	$A$	3.25	$mV$
Lumped repröf sum of excdelays	$a$	100	$Hz$
Inh. max. amplitude / $e$	$B$	22	$mV$
Lumped repröf sum of inhdelay	$b$	50	$Hz$

**Table 2.2:** Parameters of the PSP Blocks

Excitatory impulse response:

$$h_e(t) = \begin{cases} Aate^{-at} & t \geq 0 \\ 0 & t < 0 \end{cases} \quad (2.2)$$

Inhibitory impulse response:

$$h_i(t) = \begin{cases} Bbte^{-bt} & t \geq 0 \\ 0 & t < 0 \end{cases} \quad (2.3)$$

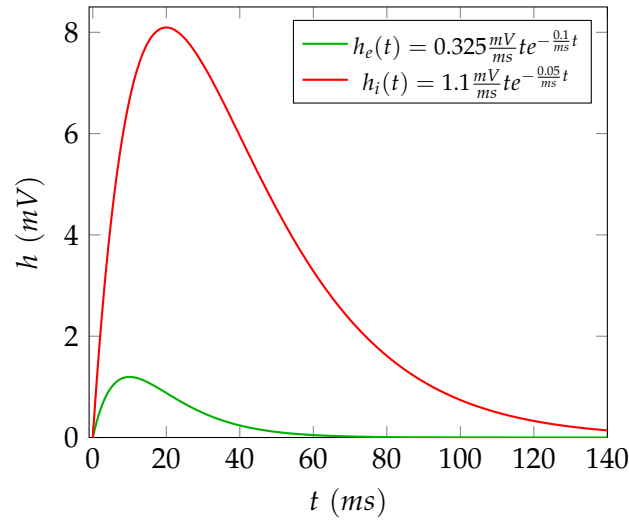


**Figure 2.4: Impulse Response Functions:** Note the small EPSP (Eq. 2.2) and the large IPSP (Eq. 2.3) [5]

Jansen and Rit [5] justify the difference in amplitude by referencing Lopes da Silva et al. [3] and stating that inhibitory neurons synapse closer to the somata of pyramidal cells (often on the cell body) than excitatory cells, increasing the effect of an inhibitory neuron about 10-fold.

☰ Todo maybe go more into detail about the reasons for stronger inhibition

The output of the Linear System defined by the PSP-Blocks is calculated by a convolution (denoted by  $*$ ) of the incoming impulse density  $x(t)$  with the impulse response function  $h(t)$  (Eq. 2.4).

**Remark** (Convolution). *The convolution of two functions  $f(t)$  and  $g(t)$  is defined as the integral of their product after one function has been reversed and shifted<sup>1</sup>:*

$$f(t) * g(t) = \int_{-\infty}^{+\infty} f(\tau)g(t - \tau)d\tau$$

If  $f(t)$  is a unit-impulse  $\delta(t)$  (in our case that would mean each cell of the previous population firing a single action potential at the same time) the result is just  $g(t)$  (in our case representing a single full-amplitude impulse response as the mean

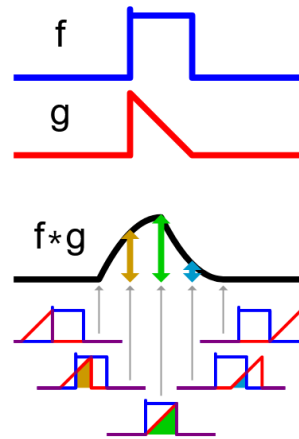


**Figure 2.5: Convolution:** The area enclosed by  $f(\tau)$  and  $g(t - \tau)$  is the value of  $(f * g)(t)$ .

<sup>1</sup>There is a very intuitive explanation of convolutions by Kalid Azad on his website <https://betterexplained.com/articles/intuitive-convolution/>.  
By Cmglee - Own work, CC BY-SA 3.0  
<https://commons.wikimedia.org/w/index.php?curid=20206883>



membrane potential):

$$\delta(t) * g(t) = \int_{-\infty}^{+\infty} \delta(\tau) g(t - \tau) d\tau = g(t)$$

In the general case, this process can be used to mathematically model the integration of incoming action potential densities in the soma.

Importantly, the Convolution Theorem states that the convolution of  $f(t)$  and  $g(t)$  becomes a simple multiplication when applying the Laplace Transform:

$$\mathcal{L}\{f(t) * g(t)\} = \mathcal{L}\{f(t)\} \mathcal{L}\{g(t)\} = F(s)G(s)$$

That means you can calculate a convolution with the inverse Laplace-Transform of the multiplication of the functions' individual Laplace-Transforms:

$$f(t) * g(t) = \mathcal{L}^{-1}\{F(s)G(s)\}$$

Since the convolution in the time-domain is a computationally heavy operation, it is oftentimes faster to transform the equation into the Laplace-Domain (see Eq. 2.5), apply the Convolution Theorem and perform the multiplication there, and transform the results back to the time-domain. This results in a second order differential equation (Eq. 2.6) that can be efficiently solved by numerical integration. To obtain this form, we need the Laplace transform  $H_e(s)$  (in this context also called *Transfer Function*) of our response function  $h_e(t)$ :

$$H_e(s) = \mathcal{L}\{h_e(t)\} = \mathcal{L}\{Aate^{-at}\} = \frac{Aa}{(s+a)^2} = \frac{Aa}{s^2 + 2as + a^2}$$

With that, we can start to transform our initial equation into the desired Second Order System:

$$\overbrace{y(t)}^{\text{PSP}} = \overbrace{h_e(t)}^{\text{impulse response}} * \overbrace{x(t)}^{\text{impulse density}} \quad (2.4)$$

applying the Laplace-Transform eliminates the convolution:

$$\begin{aligned} \xLeftrightarrow{\mathcal{L}} \quad Y(s) &= \overbrace{H_e(s)}^{\text{transfer function}} \cdot X(s) \\ \iff Y(s) &= \frac{AaX(s)}{s^2 + 2as + a^2} \\ \iff (s^2 + 2as + a^2)Y(s) &= AaX(s) \\ \iff s^2Y(s) + 2asY(s) + a^2Y(s) &= AaX(s) \end{aligned} \quad (2.5)$$

reversing the Laplace-Transform yields a differential equation in the time domain:

$$\begin{aligned} \xLeftrightarrow{\mathcal{L}^{-1}} \quad \ddot{y}(t) + 2a\dot{y}(t) + a^2y(t) &= Aax(t) \\ \iff \ddot{y}(t) &= Aax(t) - 2a\dot{y}(t) - a^2y(t) \end{aligned} \quad (2.6)$$

which can be expressed as a system of two coupled first order equations:

$$\dot{y}(t) = z(t) \quad (2.7)$$

$$\dot{z}(t) = Aax(t) - 2az(t) - a^2y(t) \quad (2.8)$$

where  $y(t)$  is the resulting PSP and  $x(t)$  the incoming pulse density. This works analogously for the inhibitory case with  $h_i(t)$ .

### 2.3.1.3 Full Linear System

Taking the two first order equations for  $\dot{y}(t)$  (Eq. 2.7) and  $\dot{z}(t)$  (Eq. 2.8), and the Block diagram (Fig. 2.6) as a base, we can now state the equations for the full Jansen-Rit Model with it's three populations. Each PSP-Block  $h(t)$  needs it's own system of coupled differential equations. The value of  $x(t)$  can be easily taken from the Block Diagram.  $y_0(t)$  is the EPSP received by both the EIN and IIN population, while  $y_1(t)$  is the EPSP and  $y_2(t)$  the IPSP received by the PC population:

$$\begin{aligned} \dot{y}_0(t) &= z_0(t) \\ \dot{z}_0(t) &= Aa\text{Sigm}[y_1(t) - y_2(t)] - 2az_0(t) - a^2y_0(t) \\ \dot{y}_1(t) &= z_1(t) \\ \dot{z}_1(t) &= Aa(p(t) + C_2\text{Sigm}[C_1y_0(t)]) - 2az_1(t) - a^2y_1(t) \\ \dot{y}_2(t) &= z_2(t) \\ \dot{z}_2(t) &= Bb(C_4\text{Sigm}[C_3y_0(t)]) - 2bz_2(t) - b^2y_2(t) \end{aligned} \quad (2.9)$$

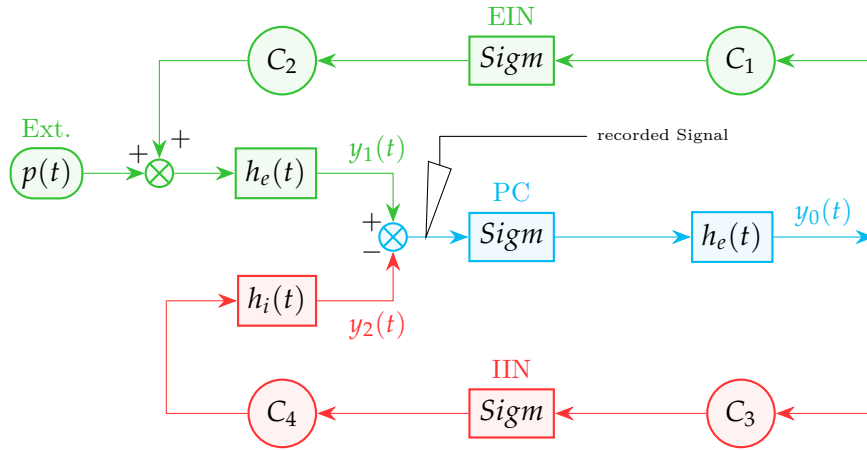


**Figure 2.6:** Colored Block diagram, visualizing the components of (Eq. 2.9)

#### 2.3.1.4 Connectivity Constants

A sensible choice for the Connectivity Constants  $C_1$  to  $C_4$  was determined by Jansen and Rit empirically by defining a histologically motivated relationship between them ( $C = C_1 = \frac{C_2}{0.8} = \frac{C_3}{0.25} = \frac{C_4}{0.25}$ ) and varying  $C$  until the system produced the desired natural alpha-like activity at  $C = C_1 = 135 \Rightarrow C_2 = 108; C_3 = C_4 = 33.75$ . Varying  $C$  can account for common synaptic phenomena like neurotransmitter depletion [6].

**Todo** go more into detail about the biological motivation and the effects of these constants on the generated signal

#### 2.3.1.5 Model Input

The model input  $p(t)$  represents the average activity of populations outside the modeled column that synapse on the columns PC population. Since this activity's source is so diverse, it is modeled by white noise (120-320 Hz).

**Todo** go more into detail why the input is modeled like this

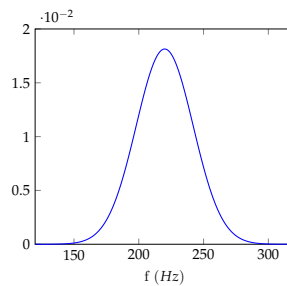


**Figure 2.7: Input distribution.** The input frequency representing  $p(t)$  is sampled from a normal distribution with  $\mu = 220$  and  $\sigma = 22$

#### 2.3.1.6 Model Output

The simulated data from  $y_1 - y_2$  while varying  $C$  looks like this:

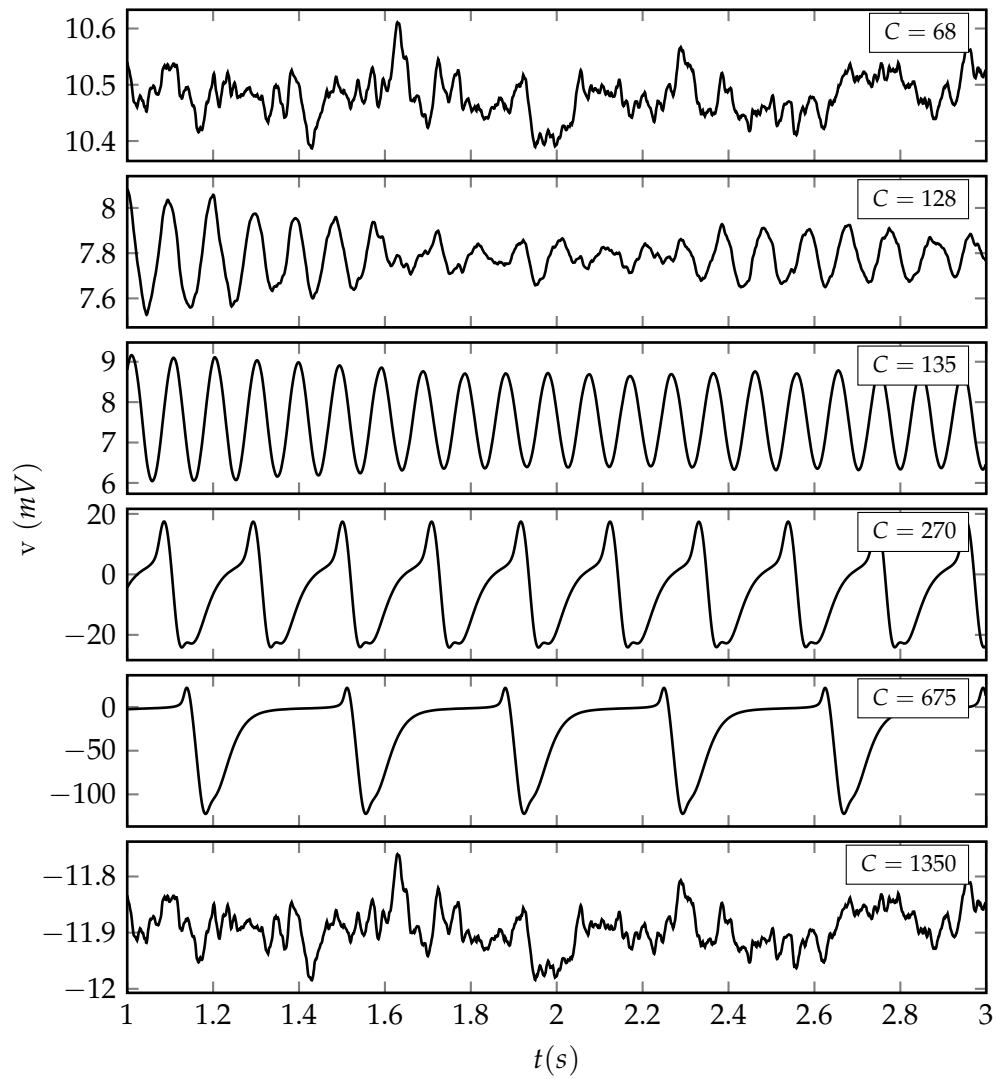


**Figure 2.8: Model Output for varying  $C$ .** Well defined alpha-activity is visible at  $C = 135$ .

☰ Todo

Explain Graph, generally provide more information to the systems output

### 2.3.2 The David and Friston Model

**⚠ Section Incomplete**

the whole David-Friston-Section is still very much preliminary

While the Jansen-Rit model succeeds in generating realistic alpha activity, real EEG Signals contain much richer spectra [9]. David and Friston [10] proposed a modification to the Jansen-Rit model, that could produce a more realistic frequency spectrum by introducing sub-populations to the model. They can be tuned individually to produce oscillations in different frequencies.

#### 2.3.2.1 Introducing sub-populations

David and Friston slightly redefine  $h(t)$  by introducing the parameters  $H$  and  $\tau$  (see Table 2.3), which is just a minor alteration of  $A$  and  $a$ .

$$h(t) = Aate^{-at} \Rightarrow h(t) = \frac{H}{\tau}te^{-\frac{1}{\tau}t}$$

Furthermore, as they are tweaking these parameters to produce slower or faster sub-populations, they define the products  $H_e\tau_e = 0.0325mVs$  and  $H_i\tau_i = 0.44mVs$  as constants. This is done to preserve the oscillatory behavior of each population [10]. When varying  $\tau$ ,  $H$  is therefore adjusted accordingly ( $H_e = \frac{0.0325mVs}{\tau_e}$ ,  $H_i = \frac{0.44mVs}{\tau_i}$ ).

Parameter		Value	Unit	Relation to [6]
Excitatory delays	$\tau_e$	0.01	s	$\tau_e = \frac{1}{a}$
Inhibitory delays	$\tau_i$	0.02	s	$\tau_i = \frac{1}{b}$
Excitatory synaptic gain	$H_e$	3.25	mV	$H_e = A$
Inhibitory synaptic gain	$H_i$	22	mV	$H_i = B$

**Table 2.3:** Parameters of the PSP Blocks after [10]

**Attention:** From now on, the indices  $[0, \dots, N]$  for  $y$ ,  $h$ ,  $\tau$  and  $H$  refer only to the subpopulations within a single population. The indices used above in the formulation for the Simple Jansen-Rit Model (and the Block Diagram) should not be confused with these. However,  $e$  and  $i$  as indices still denote excitatory and inhibitory populations respectively.

By introducing subpopulations, we split up the general impulse response function  $h(t)$  in  $N$  individual sub-functions:

$$h_n(t) = \frac{H_n}{\tau_n}te^{-\frac{1}{\tau_n}t}$$

The previously defined general PSP-Block Equation:

$$y(t) = h(t) * x(t)$$

then becomes:

$$y(t) = \sum_{n=0}^N (w_n \cdot h_n(t) * x(t)) \quad \text{with} \quad \sum_{n=0}^N w_n = 1 \quad \text{and} \quad 0 \leq w_n \leq 1$$


with N individually weighted ( $w_n$ ) and parameterized ( $h_n(t)$ ) subpopulations. We can then declare:

$$y_n(t) = h_n(t) * x(t) \quad \text{and} \quad y(t) = \sum_{n=0}^N (w_n y_n)$$

which produces the following differential equations for a single PSP Block:

$$\begin{aligned} \dot{y}_0(t) &= z_0(t) \\ \dot{z}_0(t) &= \frac{H_0}{\tau_0} x(t) - \frac{2}{\tau_0} z_0(t) - \left(\frac{1}{\tau_0}\right)^2 y_0(t) \\ &\dots \\ \dot{y}_N(t) &= z_N(t) \\ \dot{z}_N(t) &= \frac{H_N}{\tau_N} x(t) - \frac{2}{\tau_N} z_N(t) - \left(\frac{1}{\tau_N}\right)^2 y_N(t) \\ y(t) &= w_1 y_1 + \dots + w_N y_N \end{aligned} \tag{2.10}$$

David and Friston further propose an example with two subpopulations for each population with the following parameters:  $\tau_{e_1} = 10.8ms$ ,  $\tau_{i_1} = 22ms$ ,  $\tau_{e_2} = 4.6ms$ ,  $\tau_{i_2} = 2.9ms$ . While the kinetics for the first subpopulation were still close to those of the original populations ( $\tau_e = 10ms$ ,  $\tau_i = 20ms$ , which produce alpha activity), the second population's parameters were chosen to produce gamma activity.

 **Todo** put the values in a table

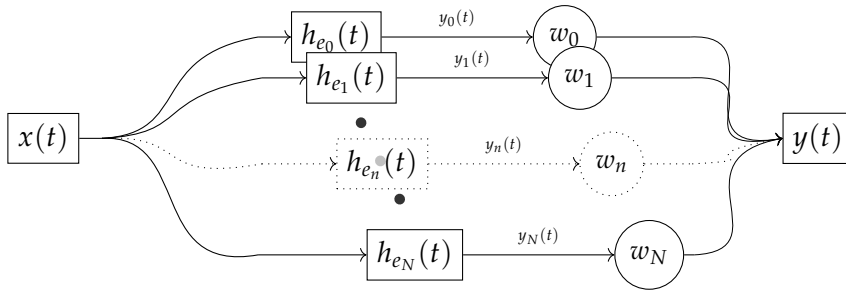


**Figure 2.9:** Example of subpopulations ( $h_{e_0}(t), \dots, h_{e_N}(t)$ ) forming an excitatory population  $h_e(t)$

### 2.3.3 New PSP Functions

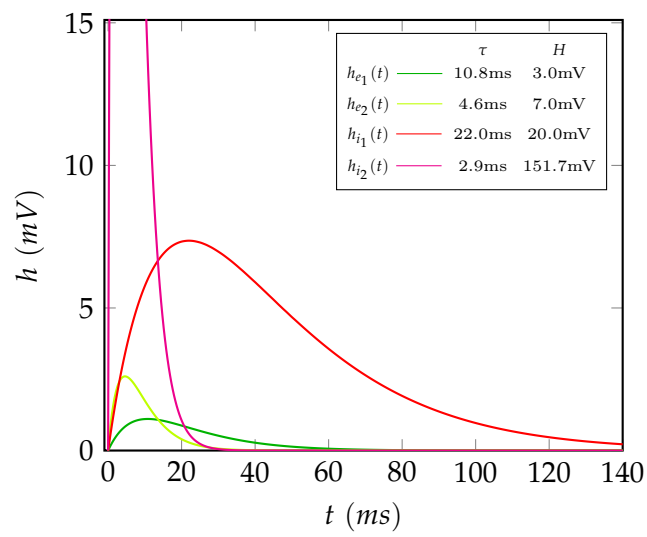


**Figure 2.10: PSP functions for Subpopulations:** — and — are faster subpopulations





## Chapter 3

# Methodology

### 3.1 PyRates Framework

**⚠ Section Incomplete**  
preliminary

The whole PyRates section is still very much

The PyRates Framework is a Python software framework, written by Richard Gast and Daniel Rose at the Max-Planck-Institute in Leipzig. It can simulate a wide range of graph-representable neural models, while setting a focus on rate-based population models [24]. It wraps computational backends like Numpy and Tensorflow and offers predefined nodes and edges (components that model units like cells or cell populations and the connections between them with mathematical equations) to be used, replaced or extended with custom equations. Furthermore it provides two simple ways to define these components and the derived network configurations: either by YAML-File or within Python code. These configurations are then compiled into optimized executable code with respect to the chosen backend before being executed. It comes with pre-configured model-definitions for some of the most frequently used models, e.g. the basic Jansen-Rit Circuit [6] and the Montbrio-Model [20], as well as some variations thereof. It's ease of use, the fact that it could easily reproduce the characteristics of the basic Jansen-Rit model out of the box, and the open-source character made it a sensible choice for this thesis.

### 3.1.1 Network Representations

#### 3.1.1.1 YAML Representation

```

1 JansenRitSynapse: # name of the template
2   description: ... # optional descriptive text
3   base: OperatorTemplate # parent template or Python class to use
4   equations: # unordered list of equations
5   - 'd/dt * V = V_t'
6   - 'd/dt * V_t = h/tau * r_in - (1./tau)^2 * V - 2.*1./tau*V_t'
7   - 'd/dt * V_t = h/tau * r_in - (1./tau)^2 * V - 2.*1./tau*V_t'
8   variables: # additional information to define variables in equations
9     r_in:
10       default: input # defines variable type
11     V:
12       default: output
13     V_t:
14       description: integration variable # optional
15       default: variable
16     tau:
17       description: Synaptic time constant
18       default: constant
19     h:
20       default: constant

```

Figure 3.1: Example YAML Synapse

```

1 JansenRitCircuit:
2   base: CircuitTemplate
3   nodes: # list nodes and label them
4     EIN: ExcitatoryInterneurons
5     IIN: InhibitoryInterneurons
6     PC: PyramidalCellPopulation
7   edges: # assign edges between nodes
8   # [<source>, <target>, <template_or_operators>, <values>]
9   - [PC/PRO/r_out, IIN/RPO_e/r_in, null, {weight: 33.75}]
10  - [PC/PRO/r_out, EIN/RPO_e/r_in, null, {weight: 135.}]
11  - [EIN/PRO/r_out, PC/RPO_e/r_in, null, {weight: 108.}]
12  - [IIN/PRO/r_out, PC/RPO_i/r_in, null, {weight: 33.75}]

```

Figure 3.2: Example YAML Circuit

### 3.1.1.2 Python Representation

```

1 from pyrates.frontend import OperatorTemplate
2 from copy import deepcopy
3
4 pro = OperatorTemplate(
5     name='PRO', path=None,
6     equations=[
7         #  $R_{out} = \frac{2e_0}{1 + e^{r(v_0 - v)}}$ 
8         "rate_out = 2.*e_0 / (1 + exp(r*(v_0 - v)))",
9     variables={
10         'rate_out': {'default': 'output'}, # output pulse density  $m_{out}$ 
11         'v': {'default': 'input'}, # incoming avg. membrane potential  $v$ 
12         'v_0': {'default': 6e-3}, # avg. firing thresh.  $v_0 = 6mV$ 
13         'e_0': {'default': 2.5}, # half of max. firing rate  $e_0 = 2.5Hz$ 
14         'r': {'default': 560.0}}, # sigmoidal steepness  $r = 560V^{-1}$ 
15     description="sigmoidal potential-to-rate operator")
16
17 rpo_e = OperatorTemplate(
18     name='RPO_e', path=None,
19     equations=[
20         #  $\dot{y}(t) = z(t)$ 
21         'd/dt * y = z',
22         #  $\dot{z}(t) = \frac{H}{\tau}x(t) - \frac{2}{\tau}z(t) - \frac{1}{\tau}y(t)$ 
23         'd/dt * z = H/tau * x - 2 * z/tau - y/tau^2',
24     variables={
25         'y': {'default': 'output'}, # output membrane potential  $y(t)$ 
26         'z': {'default': 'variable'}, # helper variable  $z(t) = \dot{y}(t)$ 
27         'x': {'default': 'input'}, # incoming pulse density  $x(t)$ 
28         'tau': {'default': 0.01}, # exc. delays  $\tau_e = 0.01s$ 
29         'H': {'default': 0.00325}}, # exc. synaptical gain  $H_e = 3.25mV$ 
30     description="excitatory rate-to-potential operator")
31
32 rpo_i = deepcopy(rpo_e).update_template(
33     name='RPO_i', path='',
34     variables={
35         'tau': {'default': 0.02}, # inh. delays  $\tau_i = 0.02s$ 
36         'H': {'default': 0.022}}, # inh. synaptical gain  $H_i = 22mV$ 
37     description="inhibitory rate-to-potential operator")
38

```

Figure 3.3: Python Example for the relevant Operators

### 3.1.2 Implementation of the Jansen-Rit Model

PyRates works with population models by compositing multiple operators, like the PSP- (or Rate-To-Potential-) and Sigmoid- (or Potential-To-Rate) Block into nodes. These nodes represent populations that can then be connected via edges (synapses). For example one might combine two PSP-Blocks (for excitatory and inhibitory input respectively) with a Sigmoid Block to create a PC-Node. This node can then receive

rate-input to each of it's PSP-Blocks and produces rate-output from it's Sigmoid-Block. The EIN- and IIN- nodes are functionally identical and just combine an excitatory PSP-Block with a Sigmoid Block. By connecting these Blocks (see Fig. 3.4) and adding random input to the excitatory PSP-Block of the PC-Node, the simple Jansen-Rit Circuit is already complete.

$$\begin{aligned}
 \frac{d}{dt}PSP_{EIN} &= PSP_{t_{EIN}} \\
 \frac{d}{dt}PSP_{t_{EIN}} &= \frac{H_e}{\tau_e} \cdot C_1 \text{Sigm}[PSP_{PC}] - \frac{2}{\tau_e} \cdot PSP_{t_{EIN}} - \left(\frac{1}{\tau_e}\right)^2 \cdot PSP_{EIN} \\
 \frac{d}{dt}PSP_{IIN} &= PSP_{t_{IIN}} \\
 \frac{d}{dt}PSP_{t_{IIN}} &= \frac{H_i}{\tau_e} \cdot C_3 \text{Sigm}[PSP_{PC}] - \frac{2}{\tau_e} \cdot PSP_{t_{IIN}} - \left(\frac{1}{\tau_e}\right)^2 \cdot PSP_{IIN} \\
 \frac{d}{dt}PSP_{PC_E} &= PSP_{t_{PC_E}} \\
 \frac{d}{dt}PSP_{t_{PC_E}} &= \frac{H_e}{\tau_e} \cdot (p(t) + C_2 \text{Sigm}[PSP_{EIN}]) - \frac{2}{\tau_e} \cdot PSP_{t_{PC_E}} - \left(\frac{1}{\tau_e}\right)^2 \cdot PSP_{PC_E} \\
 \frac{d}{dt}PSP_{PC_I} &= PSP_{t_{PC_I}} \\
 \frac{d}{dt}PSP_{t_{PC_I}} &= \frac{H_i}{\tau_i} \cdot C_4 \text{Sigm}[PSP_{IIN}] - \frac{2}{\tau_i} \cdot PSP_{t_{PC_I}} - \left(\frac{1}{\tau_i}\right)^2 \cdot PSP_{PC_I} \\
 PSP_{PC} &= PSP_{PC_E} - PSP_{PC_I}
 \end{aligned} \tag{3.1}$$

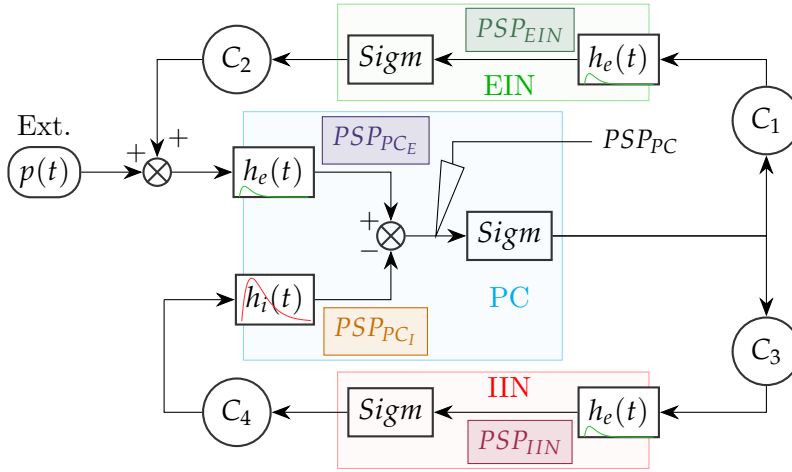


**Figure 3.4: Jansen-Rit Block Diagram as implemented in PyRates:** Each population can be clearly identified by one or more afferent PSP-Blocks and a single Sigmoid that calculates the populations output. This approach is more modular and simplifies conceptual understanding while staying mathematically equivalent. However, due to the explicit fourth PSP-Block it gives up the performance boost.

**Todo** possibly the backend-graph-optimization takes care of this? maybe check this later on...

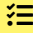
```

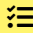
1 rpo_e = OperatorTemplate(
2     name='RPO_e', path=None,
3     equations=[
4         #-----
5         # Subpopulation 0:  $h_0(t)$ 
6         #  $\dot{y}_0 = z_0$ 
7         'd/dt * y_0 = z_0',
8         #  $\dot{z}_0 = \frac{H_0}{\tau_0} x - \frac{2}{\tau_0} z_0 - \frac{1}{\tau_0} y_0^2$ 
9         'd/dt * z_0 = H_0/tau_0 * x - 2./tau_0 * z_0 - (1./tau_0)^2. * y_0',
10        #-----
11        # Subpopulation 1:  $h_1(t)$ 
12        #  $\dot{y}_1 = z_1$ 
13        'd/dt * y_1 = z_1',
14        #  $\dot{z}_1 = \frac{H_1}{\tau_1} x - \frac{2}{\tau_1} z_1 - \frac{1}{\tau_1} y_1^2$ 
15        'd/dt * z_1 = H_1/tau_1 * x - 2./tau_1 * z_1 - (1./tau_1)^2. * y_1',
16        #-----
17        # Population output:
18        #  $y = \sum_{n=0}^N (w_n y_n)$ 
19        'PSP = w_0*y_0 + w_1*y_1'
20        #-----
21    ],
22    variables={
23        'PSP': {'default': 'output'},
24        **{var: {'default': 'variable'} for var in ['y_0', 'y_1', 'z_0', 'z_1']},
25        'x': {'default': 'input'},
26        'w_0': {'default': 1.0},
27        'w_1': {'default': 0.0},
28        'tau_0': {'default': tau_0},
29        'tau_1': {'default': tau_1},
30        'H_0': {'default': h_0},
31        'H_1': {'default': h_1}},
32    description="rate-to-potential operator")

```

Figure 3.5: PSP Block with two Sub-populations in PyRates

### 3.1.3 Simulating GABA-A Sedatives

 **Todo** why does the reduction of  $C$  represent inhibition of the whole system - what is the difference between thalamic regulation (natural sleep, etc) and GABA-A-receptor binding substances (sedation)?

 **Todo** do we have other ways of simulating sedatives in the system?



## Chapter 4

# Results

### 4.1 Research Results

#### 4.1.1 Units for propofol concentration

Some papers cite propofol concentrations in  $\frac{\mu\text{g}}{\text{mL}}$ , while others use  $\mu\text{M}$  (micromolar =  $\frac{\mu\text{mol}}{\text{L}}$ ). To get comparable numbers, we first need to establish the following relation for Propofol (molar mass: 178.27 g):

$$1 \frac{\mu\text{g}}{\text{mL}} \text{ Propofol} = \frac{1 \frac{\mu\text{g}}{\text{mL}}}{178.27 \frac{\text{g}}{\text{mol}}} = 5.609 \mu\text{M}$$

In this work, we will settle on  $\mu\text{M}$  and only mention values in  $\frac{\mu\text{g}}{\text{mL}}$  where they are taken from a source, but then provide the converted value as well.

#### 4.1.2 Realistic propofol concentrations during general anaesthesia (GA)

During GA, effect-site concentrations ( $c_e$ , concentration near the synaptic receptors) of propofol may easily range up to  $5 \frac{\mu\text{g}}{\text{mL}}$  ( $\approx 28 \mu\text{M}$ ). Loss of Consciousness (LOC) occurs on average at  $c_e \sim 2.0 \frac{\mu\text{g}}{\text{mL}}$  ( $\approx 11.2 \mu\text{M}$ ), while the Return of Consciousness (ROC) averages at  $c_e \sim 1.8 \frac{\mu\text{g}}{\text{mL}}$  ( $\approx 10.1 \mu\text{M}$ ). Both values may vary substantially for individual subjects. LOC has a strong tendency to occur at higher concentrations than ROC [12], [25]. Throughout GA, effect-site concentration is commonly derived from measured blood-plasma concentration ( $c_p$ ) using more or less complex Pharmacokinetic (PK)-Models (e.g. [18], [19]), as direct measurement is impractical for obvious reasons. Since our model will work with  $c_e$  directly, we will disregard this for now - however, it should be kept in mind.

#### 4.1.3 Effects of propofol on the IPSP

Research on the effect of propofol on the IPSC (Inhibitory Post-Synaptic Current) and EPSC has shown that propofol strongly affects the IPSP decay time [11], [13]. The EPSP and the amplitude of the IPSP are unaffected by propofol. Effect-site concentrations at clinically relevant levels increase the IPSP decay time significantly (e.g. around  $10 \mu\text{M}$  the decay time roughly doubles) [11].

Using the data-points from [11] and assuming a very rough manual logarithmic fit (see Fig. 4.1), the function

$$\mathcal{D}(c_e) = 0.65 * \ln((c_e/2) + 1) + 1$$

will be used to calculate the decay-time factor  $\lambda$  from a given effect-site concentration in  $\mu\text{M}$ .

As there unfortunately were only a few data-points (and none above  $10\text{ }\mu\text{M}$ , leaving a large part of the relevant parameter space empty), a computational model-fit might have over-valued those points. A visually fitted logarithmic function (assuming eventual effect saturation) seemed like a sensible choice for this use-case. However, since inter-subject variations are substantial in any case, the exact values do not matter as much as the order of magnitude.

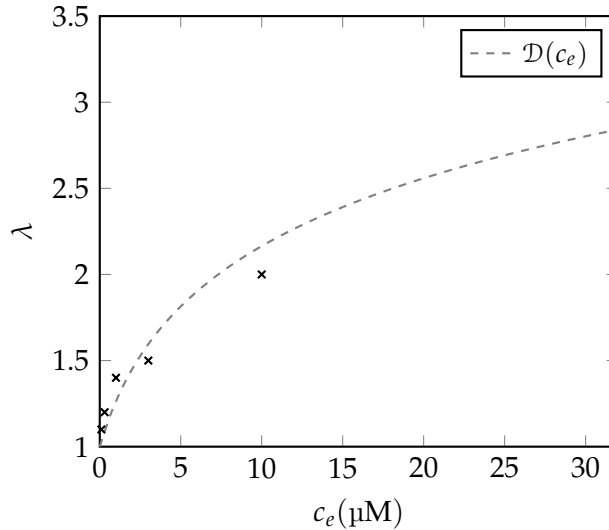


**Figure 4.1:** very rough manual logarithmic fit of decay-time factor to measured values from [11].

#### 4.1.4 Hysteresis of propofol

If the state of a system depends not only on its parameters, but also the systems history, this dependency is called hysteresis. The human body often reacts differently to the same concentration of a drug, depending on whether the concentration is rising or decaying. Hysteresis is well documented during propofol-induced GA [7], [12], [22], [25], [26]. The most prominent effect being a counter-clockwise hysteresis for LOC and ROC (as mentioned in 4.1.2). The effects on responsiveness of subjects usually start at higher concentrations than they end. While some of that effect might be caused by inaccurate PK-Models, misgauging the actual effect-site concentration, there is a growing body of research that supports the notion that the observed effect is independent of pharmacokinetic interference [15], [26].



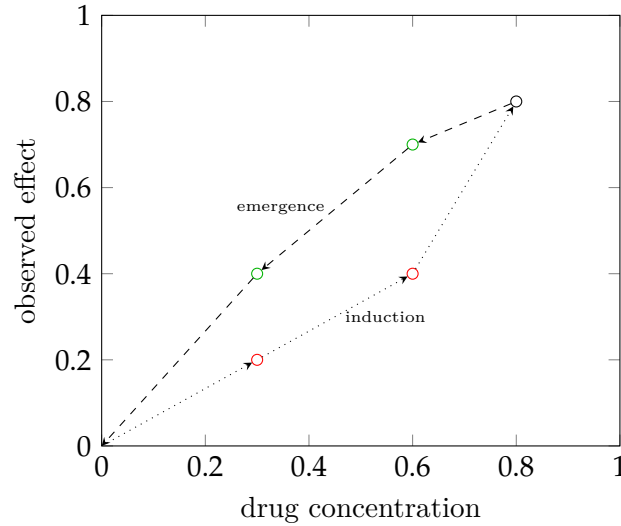


**Figure 4.2:** Example of counter-clockwise drug hysteresis

#### 4.1.5 Biphasic Effect

A biphasic effect (an initial increase of an effect, that decreases with higher concentrations) in the EEG can be observed for many sedatives [7], [8]. For propofol, a temporary steep increase in EEG amplitude in the 2–20 Hz ranges, loosely correlated with the onset of LOC, as well as ROC can be observed.

## 4.2 Simulating Propofol in the System

To simulate the effects of propofol on the GABA<sub>A</sub> receptors, the IPSP (inhibitory response function  $h_i$ ) time-constant  $\tau_i$  is increased by a factor  $\lambda$  [14]:

$$h_i(t) = \frac{H_i}{\lambda \cdot \tau_i} t e^{-\frac{1}{\lambda \cdot \tau_i}}$$

The effect of increasing  $\lambda$  for  $h_{i_1}$  and  $h_{i_2}$  is visualized in Fig. 4.3.

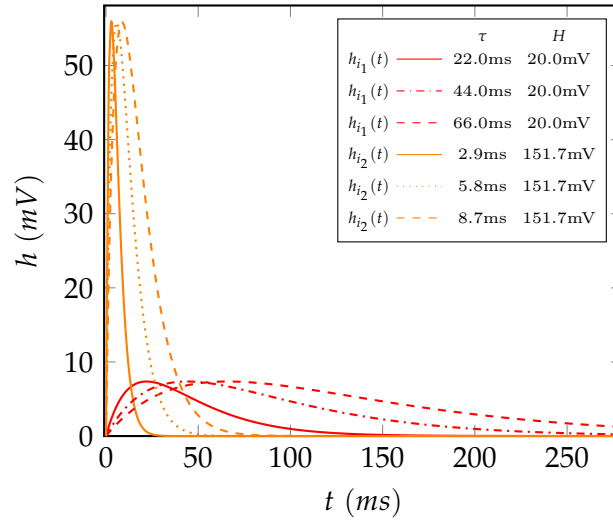


**Figure 4.3: Inhibitory PSP functions with varying  $\lambda$ :**

The duration of the effect increases while the amplitude stays constant, effectively increasing the charge transfer. ( $\lambda$  in [1.0 (no drug-effect, solid lines), 2.0 (dotted), 3.0 (dashed)])

Varying  $\lambda$  between 1 (0  $\mu\text{M}$ ) and 3.0 ( $\sim 30 \mu\text{M}$ ) appears to be a sensible choice for the clinically relevant range, given Fig. 4.1.

### 4.3 Simulating over the parameter space

When simulating over the selected parameter space  $\lambda \in [1, 3]$  (see Fig 4.4 **A**), the following phenomena can be observed:

1. Steadily increasing  $\lambda$ , from 1.0 first leads to a slight decrease in signal voltage, while roughly maintaining oscillation-amplitude (Fig 4.4 **B**). Additionally, the dominant frequencies from the 10 – 12Hz range slowly shift towards 5 – 10Hz (**C**). Overall the system appears to be in a stable state.
2. Starting from  $\lambda \sim 1.85$ , the system enters an unstable state, oscillating heavily and dramatically increasing signal amplitude and frequency amplitudes below 25 Hz. Further increasing  $\lambda$  has the same minimal effects on the disturbed signal, as the increase had before exiting the stable state.
3. At  $\lambda \sim 2.05$ , the disturbances disappear again, with the system having apparently reached a different stable state at visibly lower voltage. The dominant frequencies have jumped below 10 Hz.
4. Up to  $\lambda = 3.0$ , the signal voltage slowly continues to decrease as before, however the frequency distribution appears to have settled. Maintaining peak dosage has no further effects.
5. Decreasing from  $\lambda = 3.0$  has the expected reverse effect: only the signal voltage increases as well.
6. At  $\lambda \sim 1.95$  (somewhat lower than 2.05!), disturbances begin to form again. The system undergoes similar effects in reverse as it did in the other direction. Noteworthy is however, that the unstable state prevails until  $\lambda$  reaches  $\sim 1.48$ .

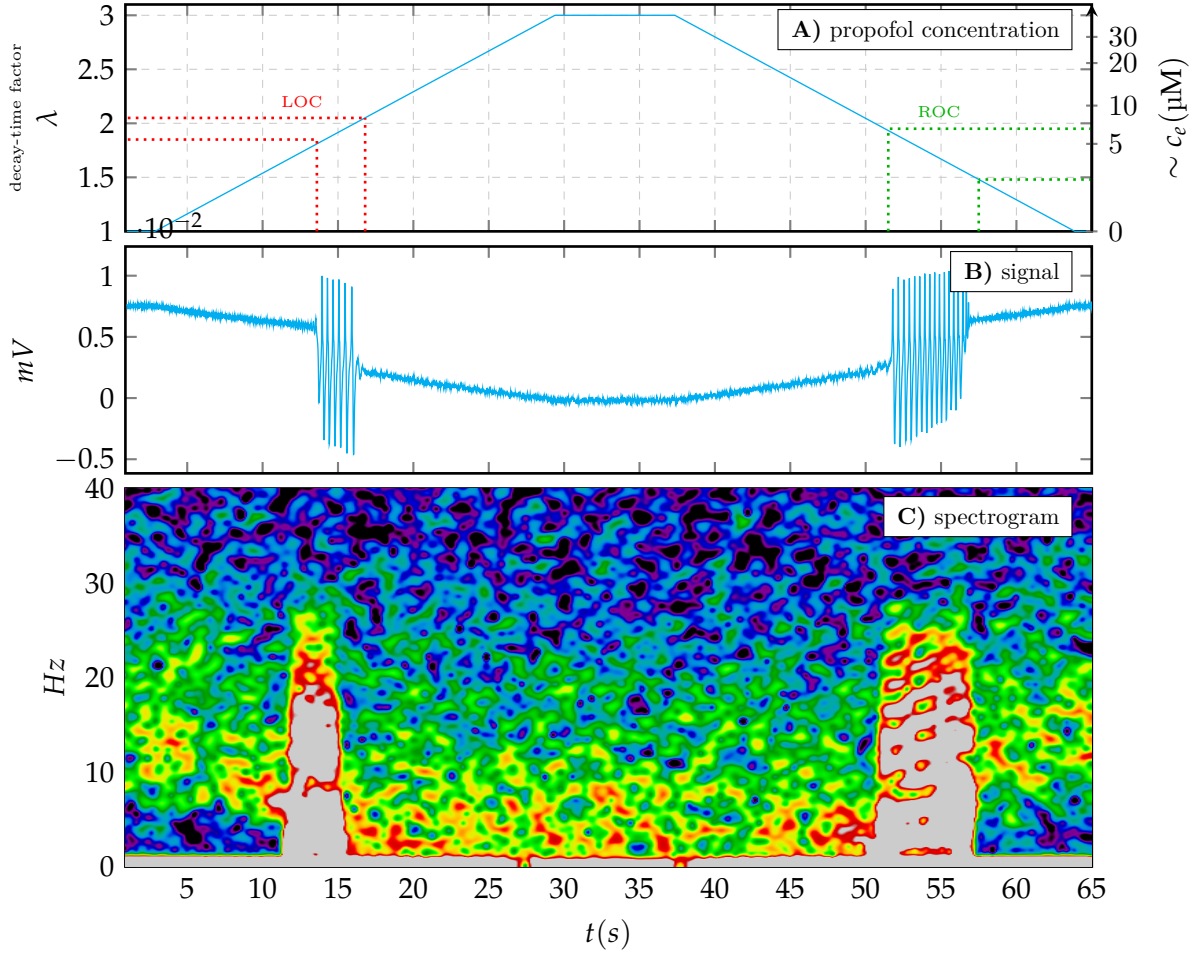


**Figure 4.4: Simulation of a sedation:**

**A):** timeline of the simulated IPSP stretch factor  $\lambda$  (roughly representing  $c_e$ )

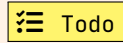
**B):** timeline of the simulated signal

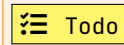
**C):** spectrogram

## 4.4 Discussion

While the NMM used for simulation is a very rough abstraction of cortical dynamics, multiple parallels to effects observed during GA can be drawn:

1. Two, distinguishable **stable states** can be observed. The frequency changes bear strong similarities to the switch to unconsciousness in GA [16], [17].
2. Induction and Emergence are asymmetrical (**hysteresis**). The system predicts that the state-change ‘LOC’ occurs at higher concentrations than ‘ROC’.
3. During state transitions, there is a strong **biphasic effect**. The system predicts that the frequency range below 25 Hz receives a temporary amplitude boost during the phase transitions, which disappears while the parameter changes continue in the same direction.
4. In the ‘unconscious’ state, frequency distribution stabilizes independent of further increasing decay-time (**slow-wave-activity saturation?** [16]).

 **Todo** elaborate on all of the above...

 **Todo** draw parallels to [15], which discusses mainly the same effects, although with a different NMM (or `mean-field-model`)

# Bibliography

- [1] H. R. Wilson and J. D. Cowan, “Excitatory and Inhibitory Interactions in Localized Populations of Model Neurons,” en, *Biophysical Journal*, vol. 12, no. 1, pp. 1–24, Jan. 1972, ISSN: 00063495. DOI: [10.1016/S0006-3495\(72\)86068-5](https://doi.org/10.1016/S0006-3495(72)86068-5). [Online]. Available: <https://linkinghub.elsevier.com/retrieve/pii/S0006349572860685> (visited on 10/23/2021).
- [2] F. H. Lopes da Silva, A. Hoeks, H. Smits, and L. H. Zetterberg, “Model of brain rhythmic activity: The alpha-rhythm of the thalamus,” en, *Kybernetik*, vol. 15, no. 1, pp. 27–37, 1974, ISSN: 0340-1200, 1432-0770. DOI: [10.1007/BF00270757](https://doi.org/10.1007/BF00270757). [Online]. Available: <http://link.springer.com/10.1007/BF00270757> (visited on 08/20/2021).
- [3] F. Lopes da Silva, A. van Rotterdam, P. Barts, E. van Heusden, and W. Burr, “Models of Neuronal Populations: The Basic Mechanisms of Rhythmicity,” en, in *Progress in Brain Research*, vol. 45, Elsevier, 1976, pp. 281–308, ISBN: 978-0-444-41457-1. DOI: [10.1016/S0079-6123\(08\)60995-4](https://doi.org/10.1016/S0079-6123(08)60995-4). [Online]. Available: <https://linkinghub.elsevier.com/retrieve/pii/S0079612308609954> (visited on 10/10/2021).
- [4] L. H. Zetterberg, L. Kristiansson, and K. Mossberg, “Performance of a model for a local neuron population,” en, *Biological Cybernetics*, vol. 31, no. 1, pp. 15–26, 1978, ISSN: 0340-1200, 1432-0770. DOI: [10.1007/BF00337367](https://doi.org/10.1007/BF00337367). [Online]. Available: <http://link.springer.com/10.1007/BF00337367> (visited on 10/10/2021).
- [5] B. H. Jansen, G. Zouridakis, and M. E. Brandt, “A neurophysiologically-based mathematical model of flash visual evoked potentials,” en, *Biological Cybernetics*, vol. 68, no. 3, pp. 275–283, Jan. 1993, ISSN: 0340-1200, 1432-0770. DOI: [10.1007/BF00224863](https://doi.org/10.1007/BF00224863). [Online]. Available: <http://link.springer.com/10.1007/BF00224863> (visited on 11/27/2020).
- [6] B. H. Jansen and V. G. Rit, “Electroencephalogram and visual evoked potential generation in a mathematical model of coupled cortical columns,” en, p. 10, 1995.
- [7] K. Kuizenga, C. J. Kalkman, and P. J. Hennis, “Quantitative electroencephalographic analysis of the biphasic concentration-effect relationship of propofol in surgical patients during extradural analgesia,” en, *British Journal of Anaesthesia*, vol. 80, no. 6, pp. 725–732, Jun. 1998, ISSN: 00070912. DOI: [10.1093/bja/80.6.725](https://doi.org/10.1093/bja/80.6.725). [Online]. Available: <https://linkinghub.elsevier.com/retrieve/pii/S0007091217403795> (visited on 05/27/2022).
- [8] K. Kuizenga, “Biphasic EEG changes in relation to loss of consciousness during induction with thiopental, propofol, etomidate, midazolam or sevoflurane,” en, p. 7, 2001.

- [9] M. Steriade, “Impact of Network Activities on Neuronal Properties in Corticothalamic Systems,” en, *Journal of Neurophysiology*, vol. 86, no. 1, pp. 1–39, Jul. 2001, ISSN: 0022-3077, 1522-1598. DOI: [10.1152/jn.2001.86.1.1](https://doi.org/10.1152/jn.2001.86.1.1). [Online]. Available: <https://www.physiology.org/doi/10.1152/jn.2001.86.1.1> (visited on 01/09/2022).
- [10] O. David and K. J. Friston, “A neural mass model for MEG/EEG:: Coupling and neuronal dynamics,” en, *NeuroImage*, vol. 20, no. 3, pp. 1743–1755, Nov. 2003, ISSN: 1053-8119. DOI: [10.1016/j.neuroimage.2003.07.015](https://doi.org/10.1016/j.neuroimage.2003.07.015). [Online]. Available: <http://www.sciencedirect.com/science/article/pii/S1053811903004579> (visited on 12/04/2020).
- [11] A. Kitamura, W. Marszalec, J. Z. Yeh, and T. Narahashi, “Effects of Halothane and Propofol on Excitatory and Inhibitory Synaptic Transmission in Rat Cortical Neurons,” en, *Journal of Pharmacology and Experimental Therapeutics*, vol. 304, no. 1, pp. 162–171, Jan. 2003, ISSN: 0022-3565, 1521-0103. DOI: [10.1124/jpet.102.043273](https://doi.org/10.1124/jpet.102.043273). [Online]. Available: <http://jpet.aspetjournals.org/lookup/doi/10.1124/jpet.102.043273> (visited on 05/26/2022).
- [12] H. Iwakiri, N. Nishihara, O. Nagata, T. Matsukawa, M. Ozaki, and D. I. Sessler, “Individual Effect-Site Concentrations of Propofol Are Similar at Loss of Consciousness and at Awakening,” en, *Anesthesia & Analgesia*, vol. 100, no. 1, pp. 107–110, Jan. 2005, ISSN: 0003-2999. DOI: [10.1213/01.ANE.0000139358.15909.EA](https://doi.org/10.1213/01.ANE.0000139358.15909.EA). [Online]. Available: <http://journals.lww.com/00000539-200501000-00021> (visited on 05/20/2022).
- [13] S. J. McDougall, T. W. Bailey, D. Mendelowitz, and M. C. Andresen, “Propofol enhances both tonic and phasic inhibitory currents in second-order neurons of the solitary tract nucleus (NTS),” en, *Neuropharmacology*, vol. 54, no. 3, pp. 552–563, Mar. 2008, ISSN: 00283908. DOI: [10.1016/j.neuropharm.2007.11.001](https://doi.org/10.1016/j.neuropharm.2007.11.001). [Online]. Available: <https://linkinghub.elsevier.com/retrieve/pii/S0028390807003516> (visited on 05/27/2022).
- [14] A. Hutt and A. Longtin, “Effects of the anesthetic agent propofol on neural populations,” en, *Cognitive Neurodynamics*, vol. 4, no. 1, pp. 37–59, Mar. 2010, ISSN: 1871-4080, 1871-4099. DOI: [10.1007/s11571-009-9092-2](https://doi.org/10.1007/s11571-009-9092-2). [Online]. Available: <http://link.springer.com/10.1007/s11571-009-9092-2> (visited on 03/22/2022).
- [15] D. A. Steyn-Ross, M. L. Steyn-Ross, J. W. Sleigh, and M. T. Wilson, “Progress in Modeling EEG Effects of General Anesthesia: Biphasic Response and Hysteresis,” en, in *Sleep and Anesthesia*, A. Hutt, Ed., New York, NY: Springer New York, 2011, pp. 167–194, ISBN: 978-1-4614-0172-8 978-1-4614-0173-5. DOI: [10.1007/978-1-4614-0173-5\\_8](https://doi.org/10.1007/978-1-4614-0173-5_8). [Online]. Available: [http://link.springer.com/10.1007/978-1-4614-0173-5\\_8](http://link.springer.com/10.1007/978-1-4614-0173-5_8) (visited on 05/26/2022).
- [16] R. Ní Mhuirheartaigh, C. Warnaby, R. Rogers, S. Jbabdi, and I. Tracey, “Slow-Wave Activity Saturation and Thalamocortical Isolation During Propofol Anesthesia in Humans,” en, *Science Translational Medicine*, vol. 5, no. 208, Oct. 2013, ISSN: 1946-6234, 1946-6242. DOI: [10.1126/scitranslmed.3006007](https://doi.org/10.1126/scitranslmed.3006007). [Online]. Available: <https://www.science.org/doi/10.1126/scitranslmed.3006007> (visited on 05/28/2022).
- [17] P. L. Purdon, E. T. Pierce, E. A. Mukamel, *et al.*, “Electroencephalogram signatures of loss and recovery of consciousness from propofol,” en, *MEDICAL SCIENCES*, p. 10, 2013.

- [18] D. J. Eleveld, J. H. Proost, L. I. Cortínez, A. R. Absalom, and M. M. R. F. Struys, “A General Purpose Pharmacokinetic Model for Propofol,” en, *Anesthesia & Analgesia*, vol. 118, no. 6, pp. 1221–1237, Jun. 2014, ISSN: 0003-2999. DOI: [10.1213/ANE.000000000000165](https://doi.org/10.1213/ANE.000000000000165). [Online]. Available: <https://journals.lww.com/00000539-201406000-00012> (visited on 05/28/2022).
- [19] Z. Liang, X. Duan, C. Su, L. Voss, J. Sleight, and X. Li, “A Pharmacokinetics-Neural Mass Model (PK-NMM) for the Simulation of EEG Activity during Propofol Anesthesia,” en, *PLOS ONE*, vol. 10, no. 12, D. Marinazzo, Ed., e0145959, Dec. 2015, ISSN: 1932-6203. DOI: [10.1371/journal.pone.0145959](https://doi.org/10.1371/journal.pone.0145959). [Online]. Available: <https://dx.plos.org/10.1371/journal.pone.0145959> (visited on 10/23/2021).
- [20] E. Montbrió, D. Pazó, and A. Roxin, “Macroscopic Description for Networks of Spiking Neurons,” en, *Physical Review X*, vol. 5, no. 2, p. 021 028, Jun. 2015, ISSN: 2160-3308. DOI: [10.1103/PhysRevX.5.021028](https://doi.org/10.1103/PhysRevX.5.021028). [Online]. Available: <https://link.aps.org/doi/10.1103/PhysRevX.5.021028> (visited on 01/09/2022).
- [21] M. M. Sahinovic, M. M. R. F. Struys, and A. R. Absalom, “Clinical Pharmacokinetics and Pharmacodynamics of Propofol,” en, *Clinical Pharmacokinetics*, vol. 57, no. 12, pp. 1539–1558, Dec. 2018, ISSN: 0312-5963, 1179-1926. DOI: [10.1007/s40262-018-0672-3](https://doi.org/10.1007/s40262-018-0672-3). [Online]. Available: <http://link.springer.com/10.1007/s40262-018-0672-3> (visited on 05/20/2022).
- [22] P. O. Sepúlveda, E. Carrasco, L. F. Tapia, *et al.*, “Evidence of hysteresis in propofol pharmacodynamics,” en, *Anaesthesia*, vol. 73, no. 1, pp. 40–48, Jan. 2018, ISSN: 00032409. DOI: [10.1111/anae.14009](https://doi.org/10.1111/anae.14009). [Online]. Available: <https://onlinelibrary.wiley.com/doi/10.1111/anae.14009> (visited on 05/26/2022).
- [23] S. Bensaid, J. Modolo, I. Merlet, F. Wendling, and P. Benquet, “COALIA: A Computational Model of Human EEG for Consciousness Research,” English, *Frontiers in Systems Neuroscience*, vol. 13, 2019, Publisher: Frontiers, ISSN: 1662-5137. DOI: [10.3389/fnsys.2019.00059](https://doi.org/10.3389/fnsys.2019.00059). [Online]. Available: <https://www.frontiersin.org/articles/10.3389/fnsys.2019.00059/full> (visited on 06/14/2020).
- [24] R. Gast, D. Rose, C. Salomon, H. E. Möller, N. Weiskopf, and T. R. Knösche, “PyRates—A Python framework for rate-based neural simulations,” en, *PLOS ONE*, vol. 14, no. 12, e0225900, Dec. 2019, Publisher: Public Library of Science, ISSN: 1932-6203. DOI: [10.1371/journal.pone.0225900](https://doi.org/10.1371/journal.pone.0225900). [Online]. Available: <https://journals.plos.org/plosone/article?id=10.1371/journal.pone.0225900> (visited on 11/27/2020).
- [25] A. L. Ferreira, R. Correia, S. Vide, *et al.*, “Patterns of Hysteresis Between Induction and Emergence of Neuroanesthesia Are Present in Spinal and Intracranial Surgeries,” en, *Journal of Neurosurgical Anesthesiology*, vol. 32, no. 1, pp. 82–89, Jan. 2020, ISSN: 0898-4921. DOI: [10.1097/ANA.0000000000000559](https://doi.org/10.1097/ANA.0000000000000559). [Online]. Available: <https://journals.lww.com/10.1097/ANA.0000000000000559> (visited on 05/27/2022).
- [26] C.-W. Su, L. Zheng, Y.-J. Li, *et al.*, “Hysteresis in anesthesia and recovery: Experimental observation and dynamical mechanism,” en, *Physical Review Research*, vol. 2, no. 2, p. 023 289, Jun. 2020, ISSN: 2643-1564. DOI: [10.1103/PhysRevResearch.2.023289](https://doi.org/10.1103/PhysRevResearch.2.023289). [Online]. Available: <https://link.aps.org/doi/10.1103/PhysRevResearch.2.023289> (visited on 05/28/2022).

- [27] C. Porcaro, I. E. Nemirovsky, F. Riganello, *et al.*, “Diagnostic Developments in Differentiating Unresponsive Wakefulness Syndrome and the Minimally Conscious State,” en, *Frontiers in Neurology*, vol. 12, p. 778 951, Jan. 2022, ISSN: 1664-2295. DOI: [10.3389/fneur.2021.778951](https://doi.org/10.3389/fneur.2021.778951). [Online]. Available: <https://www.frontiersin.org/articles/10.3389/fneur.2021.778951/full> (visited on 04/08/2022).